The Astrophysical Journal, 928:100 (11pp), 2022 April 1 https://doi.org/10.3847/1538-4357/ac53ab

Quenching of Massive Disk Galaxies in the IllustrisTNG Simulation

Yingzhong Xu (徐英中)[1], Yu Luo (於洛)[2,3,4], Xi Kang (康席)[1,2], Zhiyuan Li (李志远)[5,6], Zongnan Li (李宗男)[5,6], Peng Wang (王鹏)[7], and Noam Libeskind[7,8]
[1] Zhejiang University-Purple Mountain Observatory Joint Research Center for Astronomy, Zhejiang University, Hangzhou 310027, People's Republic of China
xuyingzhong@zju.edu.cn, kangxi@zju.edu.cn
[2] Purple Mountain Observatory, 10 Yuan Hua Road, Nanjing 210034, People's Republic of China
[3] School of Astronomy and Space Sciences, University of Science and Technology of China, Hefei 230026, People's Republic of China
[4] National Basic Science Data Center, Zhongguancun South 4th Street, Beijing 100190, People's Republic of China
[5] School of Astronomy and Space Science, Nanjing University, Nanjing 210093, People's Republic of China
[6] Key Laboratory of Modern Astronomy and Astrophysics, Nanjing University, Nanjing 210023, People's Republic of China
[7] Leibniz-Institut für Astrophysik Potsdam (AIP), An der Sternwarte 16, D-14482 Potsdam, Germany
[8] University of Lyon; UCB Lyon 1/CNRS/IN2P3; IPN Lyon (IPNL), France
Received 2021 September 8; revised 2022 February 5; accepted 2022 February 8; published 2022 March 30

Abstract

A rare population of massive disk galaxies have been found to invade the red sequence dominated by early-type galaxies. The formation and origins of these red/quenched massive disk galaxies have recently gained great interest. The quenching mechanisms that are usually proposed, such as bar quenching and environment quenching, do not seem to be suitable for those bulgeless quenched disks in a low-density environment. In this paper, we use the TNG300 simulation to investigate the formation of massive quenched central disk galaxies. It is found that these galaxies contain less gas than their star-forming counterparts and harbor giant super massive black holes (SMBHs; above $10^8\ M_\odot$). By tracing their formation history, we found that quenched disk galaxies formed early and preserved disk morphology for cosmological timescales. They have experienced less than one major merger on average, and mini-mergers (mass ratio $<1/10$) have mainly contributed to the growth of their SMBHs. In the IllustrisTNG simulation, the black hole feedback mode switches from thermal to kinetic feedback when the black hole mass is more massive than $\sim 10^8\ M_\odot$, which is more efficient to eject gas outside of the galaxy and to suppress further cooling of the hot gaseous halo. We conclude that the dominant quenching mechanism in massive red/quenched disk galaxies is kinetic active galactic nuclei feedback.

Unified Astronomy Thesaurus concepts: Galaxy evolution (594); Super massive black holes (1663); Galaxy quenching (2040); Galaxy disks (589)

1. Introduction

Our knowledge of galaxy formation has greatly benefited from large sky surveys, such as SDSS (York et al. 2000), which have provided a large sample of galaxies across a wide range of masses, morphologies, and environments. These rich data allows us to infer the statistical properties of galaxy population (e.g., Kauffmann et al. 2003a), among which the most distinct feature is the bimodal distribution of galaxy population in the color–magnitude or morphology-mass diagram (e.g., Blanton et al. 2003; Schawinski et al. 2014). This bimodality states that there are two main branches of galaxy population: the first is the red sequence, which consists of passive, bulge-dominated massive galaxies; while the second is the blue sequence, which consists of star-forming, disk-dominated low-mass galaxies.

Reproducing the two distinct sequences of galaxy population from theoretical modeling is not easy. In particular, the quenching of massive galaxies has long been the main motivation of semianalytical model (e.g., Benson et al. 2003; Croton et al. 2006; Kang et al. 2006) hydro-dynamical simulations (e.g., Vogelsberger et al. 2014a). Although the physics of quenching in detail are still unclear, it is commonly believed that the quenching of massive galaxies is related to the central SMBHs. Frequent mergers, especially major mergers, lead to the formation of a galaxy bulge (Toomre & Toomre 1972) and strong torque on the gas can lead to rapid feeding of the black hole at the center. The strong feedback from the high-accretion state of the black hole (QSO phase) can effectively sweep up the cold gas from the galaxy (e.g., Di Matteo et al. 2005), and subsequent feedback from radio active galactic nuclei (AGN; in low-accretion state) can heat the hot gas in the dark matter halo, which suppresses the further cooling of fresh gas for a cosmological timescale (e.g., Springel et al. 2005a). This merger-driven formation scenario for growth of both galaxy bulge and SMBH fits well with the observed galaxy bulge-black hole mass relation (e.g., Kormendy & Gebhardt 2001). It has been implemented , though differing significantly in detail, in the semianalytical model (e.g., Kauffmann & Haehnelt 2000; Bower et al. 2006; Croton et al. 2006; Kang et al. 2006; Somerville et al. 2008; Cattaneo et al. 2009) and the state-of-the-art hydro-dynamical simulation of galaxy formation (e.g., Sijacki et al. 2007; Hopkins et al. 2008; Vogelsberger et al. 2014b; Schaye et al. 2015; Pillepich et al. 2018a) to well reproduce the red sequence of galaxies. However, more recent evidence from both observations (e.g., Ghosh et al. 2008; Greene et al. 2010; Cisternas et al. 2011; Jiang et al. 2011; Schawinski et al. 2011; Simmons et al. 2011; Kocevski et al. 2012; Schawinski et al. 2012; Simmons et al. 2013; Bizzocchi et al. 2014; Kaviraj 2014; Simmons et al. 2017; Smethurst et al. 2019; Bohn et al. 2020; Smethurst et al. 2021) and simulations (e.g., Martin et al. 2018; McAlpine et al. 2020) have found that SMBHs and AGN activities are also seen in

disk-dominated galaxies. This suggests that secular processes other than major mergers, such as minor mergers and smooth gas accretion, may also play a role in driving the growth of both SMBHs and galaxies.

In addition to the dominant population of early-type galaxies at the massive end ($>10^{10}$ $M_{\odot}$) of the red sequence, a rare population of disk galaxies also intrude the red sequence at the massive end. The red disk galaxy population has attracted great attention recently (e.g., Zhang et al. 2019; Zhou et al. 2021b; Zhang et al. 2021; Xu et al. 2021). In fact, red disk galaxies have been known for several decades (e.g., van den Bergh 1976; Couch et al. 1998). It has been found that most red disk galaxies are really passive and their star formation has been quenched (e.g., Tojeiro et al. 2013; Guo et al. 2020). Most red disks preferentially reside in intermediate/high density regions and they also show distinct sign of bars (e.g., Masters et al. 2010; Hao et al. 2019; Mahajan et al. 2020; Zhou et al. 2021a).

The formation and quenching mechanism of a red disk galaxy is still not clear. It is widely speculated that both the internal structure and external environment could lead to the quenching of a red disk (e.g., Fraser-McKelvie et al. 2018). Red disks with significant bars are quenched by internal process, such as bar quenching, while those in high/intermediate environment density may be quenched due to the environment effect, such as ram pressure stripping or strangulation. However, such quenching mechanisms may not apply to recent findings of massive disk galaxies lacking clear signature of bar and in low-density environment (Luo et al. 2020; Xu et al. 2021). For these galaxies, some additional quenching mechanisms have to be invoked, such as the suppression of cooling from the hot gaseous halo (e.g., Man & Belli 2018). AGN feedback is a very natural choice. However, strong AGN feedback, under the merger-driven paradigm, does not seem to be applicable in massive bulgeless galaxies because they are not expected to possess giant SMBHs. However, some recent observations confirm the presence of a strong AGN in massive disk-dominant galaxies (e.g., Greene et al. 2010; Cisternas et al. 2011; Bizzocchi et al. 2014) and even in the massive bulgeless galaxies (e.g., Ghosh et al. 2008; Schawinski et al. 2011; Kocevski et al. 2012; Simmons et al. 2012, 2013, 2017; Bohn et al. 2020). Interestingly, it was the finding of these merger-free objects that challenged the merger-driven mechanism (e.g., Greene et al. 2010; Cisternas et al. 2011; Jiang et al. 2011; Simmons et al. 2013).

Recently, Luo et al. (2020) studied the red disk galaxy using the model galaxies from the IllustrisTNG simulation (e.g., Pillepich et al. 2017; Marinacci et al. 2018). They found eight quenched disk galaxies and have shown that these galaxies have massive black hole mass ($>10^{8}$ $M_{\odot}$), about $\sim$1 dex higher than the predictions from the classical bulge mass-black hole mass relation. Luo et al. (2020) speculated that it was the AGN feedback that shut off the cooling of the hot halo gas, thus the disk galaxies are kept quenched. However, because their selection of quenched disks is limited to galaxies with stellar masses larger than 10^{11} $M_{\odot}$, the sample is too small (only eight galaxies) for statistical analysis.

In this work, we use the IllustrisTNG simulation and select quenched disk galaxies with stellar masses larger than $10^{10.5}$ $M_{\odot}$. Compared with the work of Luo et al. (2020), we have a much larger samples. This enables us to study the properties and formation history of quenched disk galaxies in more detail. In particular, we focus on the quenching mechanism of these red disk galaxies. This paper is organized as follows: in Section 2, we introduce selection of galaxy sample from the simulation and we present their properties in Section 3. We explore the evolution of gas, SMBHs and specific star formation rates in Section 4. We then analyze the growth of SMBHs in Section 5. In Section 6, we give our conclusions and will include some discussion of this topic.

2. Sample Selection

In this section, we will briefly highlight a few implementations of the IllustrisTNG simulation, which we believe are relevant to our study and our selection of model galaxy. We select two samples at $z = 0$: the first is the massive quenched central galaxies (named SampleQ), and the second is the massive star-forming central disk galaxies (named SampleF). Their comparison gives us a clue as to why some central disk galaxies are quenched while others are not.

2.1. IllustrisTNG

The IllustrisTNG (hereafter TNG)[9] project is a series of cosmological magnetohydrodynamical simulations, which have produced many wonderful results (e.g., Pillepich et al. 2017; Marinacci et al. 2018) that have improved our understanding of galaxy formation. There are three simulation boxes with three different resolutions for TNG simulations. In this work, we selected samples from the simulation TNG300-1 (Marinacci et al. 2018; Naiman et al. 2018; Nelson et al. 2018, 2019; Pillepich et al. 2018b; Springel et al. 2018) with the largest simulation box (roughly $(300\,\mathrm{Mpc})^3$) and high resolution because it could provide a large sample of massive galaxies ($M_{\star} \geqslant 10^{10.5}$ $M_{\odot}$). We have adopted the Planck Collaboration et al. (2016) best fit cosmological parameters: dark energy density $\Omega_{\Lambda} = 0.6911$, matter density $\Omega_m = 0.3089$, baryon density $\Omega_b = 0.0486$, Hubble constant $H_0 = 67.74$ kms^{-1} Mpc^{-1}, normalization $\sigma_8 = 0.8159$ and the spectral index $n_s = 0.9667$.

In the following we list some physical prescriptions of the TNG simulations that are related to our investigation:

1. *Merger history*. In the TNG simulations, galaxies live in the halos and subhalos, which are identified by using the Friends-of-Friends (FOF; Springel et al. 2001) and SUBFIND algorithms (Springel et al. 2005b). The SubLink (Rodriguez-Gomez et al. 2015) merger tree records the formation history of the galaxies. The SubLink is a algorithm that is used to link subhalos at different snapshots and to construct the merger trees. For a subhalo A with N_A member particles at snapshot S_A, it has a main progenitor and a sole descendant at $S_A - 1$ and $S_A + 1$, respectively. In general, the member particles of subhalo A at S_A are contained in different subhalos at $S_A - 1$, which are all defined to be progenitors of subhalo A. The main progenitor is defined as the one that contains the maximum number of particles belonging to subhalo A. Similarly, the descendant is defined as the halo at $S_A + 1$ that contains the maximum number of member particles belonging to subhalo A. The main progenitor and descendant is then used to construct the merger tree.

[9] https://www.tng-project.org/

For more details, we refer the reader to the paper by Rodriguez-Gomez et al. (2015).

2. *Hydrogen gas*. The gas cell is able to form stars when its hydrogen number density is above a threshold ($\sim 0.1\,\mathrm{cm}^{-3}$) according to the star formation model (Springel & Hernquist 2003), which is used in the TNG simulation. The hydrogen number density is $n_H = \frac{X_H \rho}{m_p}$, where X_H is the abundance of hydrogen, ρ is the mass density of the cell, m_p is the mass of proton. The star-forming gas ($n_H > 0.1\,\mathrm{cm}^{-3}$) which is dominated ($\gtrsim 85\%$, refer to the first figure in Springel & Hernquist 2003) by cold phase ($T = 10^3$ K) can be treated as cold gas. This follows the effective equations of state. For the non-star-forming gas ($n_H < 0.1\,\mathrm{cm}^{-3}$), it follows the ideal-gas equations of state and the temperature is at most cooled to 10^4 K (cool or hot gas).
3. *Super massive black hole*. When the mass of a FOF halo, without a SMBH, is above $\sim 7 \times 10^{10}\ M_\odot$, a SMBH seed ($\sim 10^6\ M_\odot$) is put into the center (where the potential is minimal) of the halo. There are two kinds of feedback mode for the SMBH: thermal and kinetic mode. When the black hole growth is in a high-accretion state, the feedback energy will be injected into the surrounding gas as thermal energy; while in a low-accretion state, momentum rather than thermal energy will be transmitted to the surroundings in a random direction driving a strong wind. In TNG simulations, when the mass of the SMBH $M_{\rm bh}$ exceeds $\sim 10^8\ M_\odot$ the accretion mode will switch from thermal to kinetic mode. We recommend readers who are interested in the black hole model used in the TNG to reference the paper by Weinberger et al. (2017).

2.2. Selecting Model Galaxies

We investigate the quenched massive disk central galaxies from TNG300-1 data at $z = 0$. Therefore, we use three quantities to select galaxy the sample: the stellar mass $M_\star$; the specific star formation rate, $\mathrm{sSFR} = \frac{\mathrm{SFR}}{M_\star}$(SFR represents the instantaneous star formation rate, which is a direct output in the TNG simulation); and the ratio of spheroid stellar mass to total stellar mass of galaxy, labeled as S/T.

First, we select central galaxy defined as the most massive member galaxy in a group and calculate these three quantities within $3R_e$ (R_e is the stellar half-mass–radius) relative to the center of the galaxy. The calculation of $M_\star$ and sSFR is straightforward. For $M_\star$, we summed the mass of every star particles within $3R_e$. For sSFR, we summed the SFR (the direct output of the simulation) of every gas cell within $3R_e$ and divided it by the stellar mass $M_\star$.

For S/T, we need to decompose the stellar mass into the disk and spheroid components. The classical method is photometric decomposition, which relies on the empirical assumption that the disk and bulge components of a galaxy have different surface brightness profiles. However, there are some more suitable methods than the photometric decomposition for simulation data, such as the kinematic decomposition (KD) that decomposes a galaxy according to the distribution of a characteristic quantity ϵ. There are a few definitions of ϵ (e.g., Abadi et al. 2003a, 2003b; Scannapieco et al. 2009; Doménech-Moral et al. 2012; Pillepich et al. 2017). In this work, we choose the definition of ϵ that was used in Tacchella et al. (2019). We note that there is no particular reason why we selected the method of Tacchella et al. (2019) over other methods. We only made this choice because this decomposition is faster because it does not require the potential energy of each particle to be calculated, which is required by other kinematic methods and the obtained S/T is well correlated with that from other kinematic methods, as shown by Tacchella et al. (2019). The definition that we used is $\epsilon = \frac{j_z}{j}$, where j is the angular momentum of a stellar particle and j_z is the component of angular momentum projected to the direction of total stellar angular momentum of a galaxy within $3R_e$. Consequently, the mass of the spheroid component, M_s, is twice the sum of the mass of stellar particles with $\epsilon \leqslant 0$, under the simple assumption that the bulge stars move randomly with a symmetrical distribution. We then got $S/T = \frac{M_s}{M_{\rm total}}$, here $M_{\rm total}$ is the the total mass of all the stellar particles within $3R_e$. It is noted that S/T could be larger than 1 because we simply double the stellar mass with $\epsilon \leqslant 0$; hence, we removed those galaxies with S/T > 1, which are not realistic (only $\sim 1\%$ of the total 22417 massive central galaxies in our sample). In Figure 1, we randomly chose two galaxies (shown in the first and second row) and plotted their face-on (left-hand panel) and edge-on (right-hand panel) stellar surface mass density distribution. The spheroid to total ratio (S/T) that were calculated using these KD methods are also labeled in the panels. This figure show that the methods that we used in this paper work well.

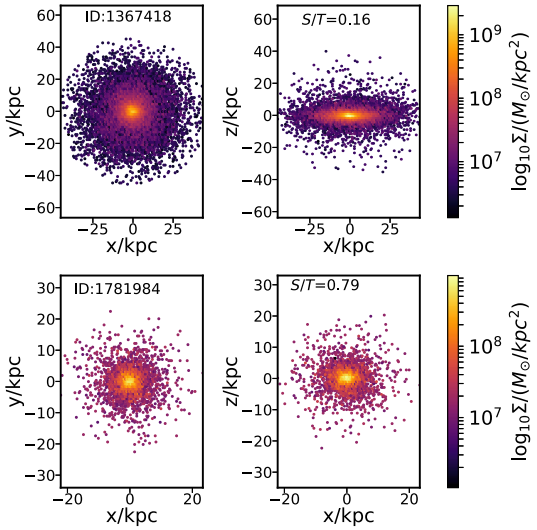

Figure 1. The top and bottom row show the face-on (left-hand panel) and edge-on (right-hand panel) stellar surface mass density distribution of two randomly selected galaxies, respectively. Their TNG ID and the spheroid to total mass ratio (S/T), calculated using the methods that we introduced, are also labeled in the panels. In each image, we only considered star particles within $6R_e$. Obviously, the KD methods that we used are able to pick out the disk galaxies.

In this work, we define a galaxy to be bulgeless if $\mathrm{S/T} < 0.25$, and a galaxy with $\mathrm{sSFR} < 10^{-11}\ \mathrm{yr}^{-1}$ to be quenched. For our purposes, we finally select two samples of galaxies: the first includes quenched disk galaxies with $M_\star > 10^{10.5}\ M_\odot$, $\mathrm{sSFR} < 10^{-11}\ \mathrm{yr}^{-1}$ and $\mathrm{S/T} < 0.25$, named SampleQ; and the second includes star-forming disk galaxies with $M_\star > 10^{10.5}\ M_\odot$, $\mathrm{sSFR} > 10^{-11}\ \mathrm{yr}^{-1}$ and $\mathrm{S/T} < 0.25$, named SampleF. From the TNG simulation, we get 545 and 658 members, respectively, for the two samples. Considering the resolution limit of the simulation, the star formation rate

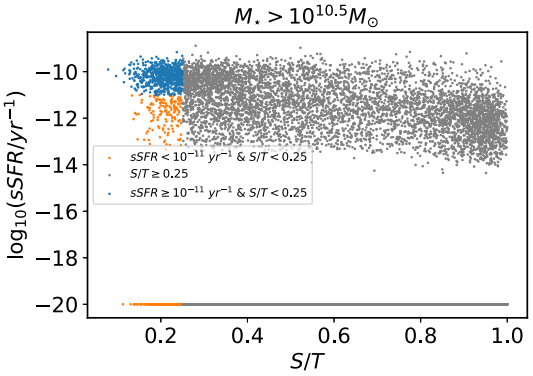

Figure 2. The S/T and sSFR distribution for massive($M_\star > 10^{10.5}\ M_\odot$) central galaxies. Blue points belong to SampleF, orange points belong to SampleQ, and gray points belong to the rest. For those galaxies with SFR $= 0\ M_\odot\ \mathrm{yr}^{-1}$, we set sSFR $= 10^{-20}\ \mathrm{yr}^{-1}$.

(SFR) will be set to 0 when the SFR is unresolved. Thus, here we set sSFR $= 10^{-20}\ \mathrm{yr}^{-1}$ when SFR $= 0\ M_\odot\ \mathrm{yr}^{-1}$.

In Figure 2 we show the distribution of TNG model galaxies on the specific star formation and morphology diagram. Here, all central galaxies with $M_* > 10^{10.5}\ M_\odot$ are shown, while the blue points are used for SampleF and orange points are used for SampleQ. In general, the simulation is consistent with the observational trend that at given mass, bulge-dominated galaxies have lower star formation rate and disk-dominated galaxies have higher star formation rate (e.g., Kauffmann et al. 2003b; Snyder et al. 2015). In the following sections, we mainly focus on disk-dominated galaxies (colored dots) and investigate why some of them are quenched and others are not.

3. The Gas Content and Black Hole of Quenched Massive Disk Galaxies

In this section, we examine the differences between SampleQ and SampleF in some physical properties, such as the gas content and the central black hole mass, because they are thought to be the main factors leading to the quenching of disk galaxies (e.g., Luo et al. 2020). Investigation of other properties, such as galaxy structure between SampleQ and SampleF, requires simulation with higher resolutions, which are not available at the moment.

3.1. The Gas Content

Both hot and cold gas are related to star formation activity in a galaxy because the former is the source of cooling and the latter is direct fuel for star formation. In Figure 3, we show the halo gas mass and halo virial mass distribution of both samples, where the total gas refers to all of the gas cell within the halo, including both cold and hot, and the halo virial mass $M_{\rm halo}$ is the total mass of a sphere inside which the mean density is 200 times the critical density. It can clearly be seen that at the fixed halo virial mass, the quenched sample (orange dots) has lower halo gas mass than the star-forming sample (blue dots), while two samples have similar halo virial mass distribution (right-hand small panel). The same phenomenon was also found by Davies et al. (2020).

Because cold gas, mainly in hydrogen, is the direct gas reservoir for star formation, in Figure 4 we show the distribution of the mass-weighted mean hydrogen gas density n_H within $3R_e$ to illustrate the cold (hydrogen) gas content. As expected, the mean hydrogen gas densities of SampleQ are

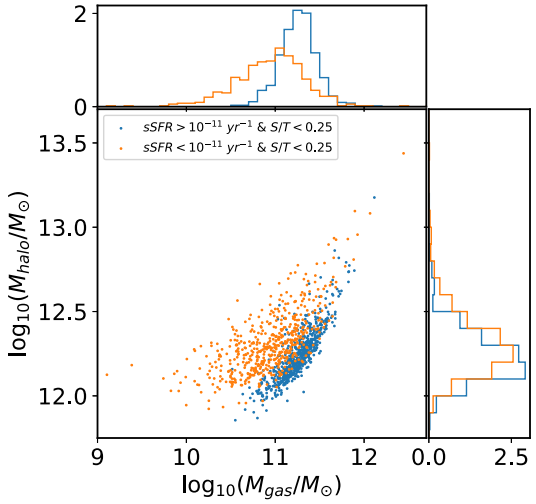

Figure 3. This scatter plot shows the relation between the halo virial mass $M_{\rm halo}$ and the gas mass $M_{\rm gas}$. The two marginal distributions are also displayed on the top and right-hand side. The orange points (i.e., quenched galaxies) have less gas than the star-forming points with similar halo virial mass.

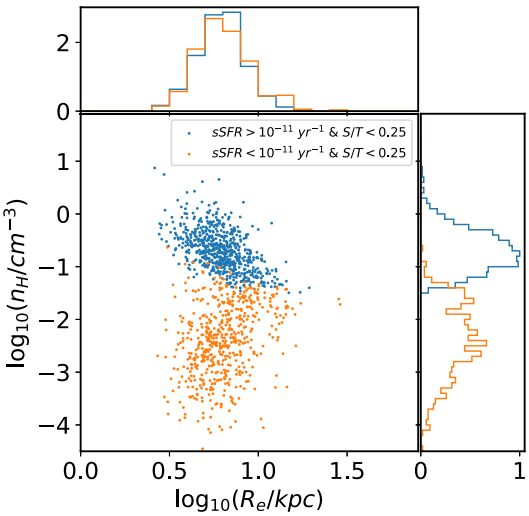

Figure 4. This figure is similar to Figure 3 except for the relationship between the mean gas density n_H and the stellar half-mass–radius R_e. Obviously, SampleQ lacks star-forming gas ($n_H > 0.1\ \mathrm{cm}^{-3}$), while their sizes ($R_e$) are similar to those of SampleF.

systematically lower than $0.1\ \mathrm{cm}^{-3}$, while those of SampleF are higher. In the TNG simulation, a gas cell is allowed to form stars only if its density, n_H, is above the threshold $0.1\ \mathrm{cm}^{-3}$. This means that SampleQ lacks hydrogen gas to form stars within $3R_e$. It is also found that the lower hydrogen gas in SampleQ is not due to their larger disk size. As seen from the upper panel, the distributions of disk size in SampleQ and SampleF are very similar.

These results show that both the total and cold gas are less in SampleQ than in SampleF. Because cold gas comes from the cooling of hot gas and the gas content of our selected sample galaxies are dominated by hot gas, the deficiency of cold gas in SampleQ is mainly due to the shortage of total gas compared to SampleF. In the following text, we do not distinguish the cold gas from the hot gas but focus instead on the total gas evolution and we also investigate which physical processes produce less total gas in SampleQ.

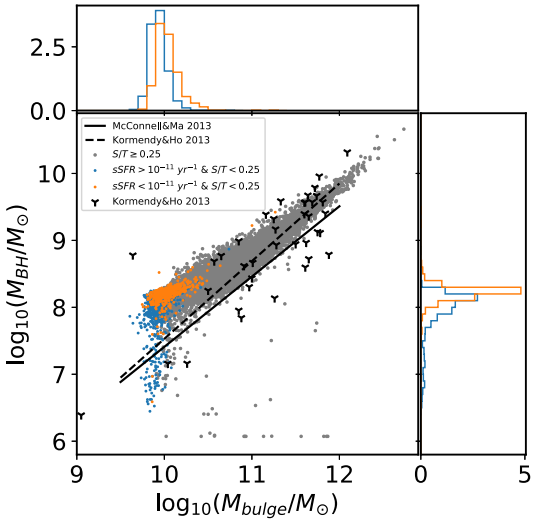

Figure 5. The relationship between black hole mass and bulge mass for massive($M_\star > 10^{10.5}$ $M_\odot$) central galaxies. Blue points belong to SampleF, orange points belong to SampleQ, gray points are the rest. SampleQ owns a more massive SMBH ($>10^8$ $M_\odot$) than SampleF with a similar bulge mass. The black mark and the solid line are quoted from Kormendy & Ho (2013), and the dashed line is quoted from McConnell & Ma (2013).

3.2. The Black Hole Mass

As mentioned earlier, a black hole is a key component of modeling in nearly all hydro-dynamical simulations. Traditionally the mass of the black hole in elliptical galaxies is measured using spectroscopic methods. It was recently found that disk galaxies follow similar black hole mass-bulge (or total) mass relation but with a different slope and a larger scatter (e.g., Davis et al. 2018, 2019). The focus of this work is not to compare the predicted black hole mass from TNG simulation with the data in detail but to gain insight into the possible effects of black hole feedback on disk quenching. For a more detailed comparison of predicted black hole mass with the data from TNG simulation, we refer the reader to a few recent works (e.g., Li et al. 2020; Terrazas et al. 2020).

Figure 5 shows the bulge-SMBH relation. It is straightforward to see that both the quenched galaxies (orange dots) and star-forming galaxies (blue dots) have similar bulge mass, while the quenched galaxies have higher black hole mass at given bulge mass. However, it is notable that the simulated galaxies lie systematically above the two classical bulge-SMBH relations (solid and dashed lines) (Kormendy & Ho 2013; McConnell & Ma 2013). We note that this deviation from the observed bulge-SMBH relation at the low-mass end is also seen in the highest resolution TNG simulation with a box size of $(30h^{-1}$ Mpc$)^3$ by Weinberger et al. (2017), who concluded that this may be a result of increasing mass of the seed black hole and the definition of the bulge mass (it is notable that they used the same definition of bulge mass as this work did, except that they considered star particles within 0.1 virial radius, $0.1R_{200}$, not the $3R_e$ we used here). However, this will not affect our conclusion that galaxies of SampleQ have systematically higher black hole mass than SampleF.

From these results, we can conclude that the galaxies of SampleQ have a larger black hole($>10^8$ $M_\odot$), and have less cold and less total gas than those of SampleF, while the two samples have similar distributions for other quantities (e.g., the halo virial mass $M_{\rm halo}$, the stellar half-mass–radius $R_{\rm e}$).

Davies et al. (2019, 2020) found a significant positive correlation between the specific star formation rate (sSFR) and the circumgalactic medium (CGM) mass fraction ($f_{\rm CGM} \equiv \frac{M_{\rm gas}}{M_{200}}$, where $M_{\rm gas}$ is the total mass of the gas cells within virial radius which are non-star-forming) for central galaxies in EAGLE (Schaye et al. 2015; Crain et al. 2015) and TNG simulations because of the lack of fuel to form stars. Their results also indicated that the low $f_{\rm CGM}$ is due to the SMBH. Particularly for TNG, the AGN feedback mode will change from thermal to kinetic when the $M_{\rm bh}$ is above the threshold ($\sim 10^8$ $M_\odot$) (Weinberger et al. 2017). In the kinetic mode, the gas can be expelled effectively from the galaxy or may even be driven out of the halo (e.g., Weinberger et al. 2018; Terrazas et al. 2020; Zinger et al. 2020).

This quenching mechanism seems to be applicable to our SampleQ, which has both lower gas in the halo and giant SMBH ($M_{\rm bh} > 10^8$ $M_\odot$). However, it is unknown why these quenched disk galaxies have higher black hole mass. It is also interesting to note that there are some galaxies with SMBHs ($\sim 10^8$ $M_\odot$) but are still star-forming. Thus, having a SMBH does not necessarily lead to the quenching of a galaxy. The answers to this problem may be behind the formation history of the galaxies and their SMBHs. In the following sections, we investigate their formation history in detail.

4. The Evolution History of Quenched Massive Disk Galaxies

We used the SubLink merger tree data of the TNG simulation (see Section 2.1) to investigate the evolution history of the gas mass $M_{\rm gas}$ and the black hole mass $M_{\rm bh}$.

We extracted the formation history for each model galaxy in our samples, which is the track along the main progenitor at each time step. In some cases, a galaxy will switch its identity from a central to a satellite, or vice versa. This is due to the shortcoming of the SUBFIND algorithm (Poole et al. 2017). So we eliminated from our original samples those galaxies (at $z = 0$) that are not always central galaxies during their lifetimes. Finally, about 38.6% and 40.7% of the members in original SampleF and SampleQ were removed, respectively.

We then obtain the halo gas mass along the main branch for each galaxy at $z = 0$ in our sample. We found that for almost all galaxies in SampleQ, their halo gas mass reached the maximum in the past at $z > 0$ and they then decrease to $z = 0$, which will soon be shown and explained more explicitly in Figure 7 (Section 4.1). So, for each galaxy in SampleQ and SampleF, we can define a new quantity, $t_{\rm max}$, as the time when the halo gas mass $M_{\rm gas}$ reaches its maximum value during the formation history. Different galaxies have different $t_{\rm max}$ and their distributions of the $t_{\rm max}$ are plotted in Figure 6.

Obviously, the $t_{\rm max}$ distribution of SampleF (blue histogram) has a sharp narrow peak at the present time ($z = 0$), while that of SampleQ (orange histogram) is very flat. This means that for most SampleF galaxies, the gas mass will keep increasing until $z = 0$; however, for most galaxies of SampleQ, the gas mass peak appears before $z = 0$.

Considering the wide distribution of $t_{\rm max}$ for SampleQ, we separated the samples into subgroups according their values of $t_{\rm max}$. We divided the $t_{\rm max}$ from $t = 4.29$ Gyr to $t = 13.8$ Gyr into 12 intervals: ([4.29, 5.12), [5.12, 5.88), [5.88, 6.69), [6.69, 7.45), [7.45, 8.28), [8.28, 9.06), [9.06, 9.84), [9.84, 10.65),

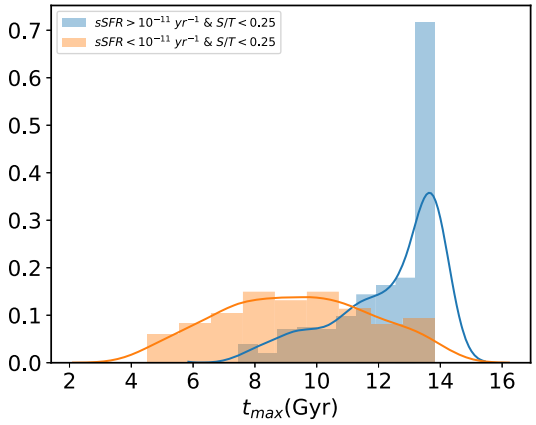

Figure 6. The distribution of $t_{\max}$ for SampleQ (orange) and SampleF (blue), respectively. Note that $t_{\max}$ is defined as the time at which the galaxy has the largest gas mass $M_{\rm gas}$ in the halo among its whole history. The blue distribution has a sharp narrow peak at the present time ($z = 0$), while the orange is very flat.

[10.65, 11.51), [11.51, 12.34), [12.34, 13.13), [13.13, 13.80][10] Gyr). Then we got 12 subsamples from SampleQ: $Q_{i,i=0,1\cdots11}$ corresponding to those time intervals (which means that subgroup Q_0 consisted of galaxies with $t_{\max} \in [4.29, 5.12)$ Gyr). The number galaxies of each subsample is 12, 14, 22, 28, 38, 31, 38, 36, 36, 24, 22, and 22, respectively. Similarly, we separated SampleF into two groups: $F_0(t_{\max} \in [7.45, 10.65)$[11] Gyr) of 70 members and $F_1(t_{\max} \in [10.65, 13.80]$[12] Gyr) of 334 members because it has a sharp $t_{\max}$ distribution.

In the following, we selected three representative subsamples of SampleQ: $Q_0(t_{\max} \in [4.29, 5.12)$ Gyr), $Q_5(t_{\max} \in [8.28, 9.06)$ Gyr), $Q_{10}(t_{\max} \in [12.34, 13.13)$ Gyr) and one subsample of SampleF: $F_1(t_{\max} \in [10.65, 13.80)$ Gyr) to investigate their evolution history because any two subsamples with close $t_{\max}$ values will have similar behaviors in their evolution.

4.1. The Evolution of the Gas Mass

We first show the evolution history of the gas mass $M_{\rm gas}$. In Figure 7, the gray, green, and light-blue dashed lines represent the three quenching subsamples: Q_0, Q_5 and Q_{10}, respectively, while the red-solid line represents the star-forming subsample: F_1. The three vertical lines indicate the median value of $t_{\max}$ (which are $t_{\max} = 4.82$ Gyr for Q_0, $t_{\max} = 8.29$ Gyr for Q_5 and $t_{\max} = 12.67$ Gyr for Q_{10}.) of the corresponding quenching subsamples(shown by the same color). The contour range represents the 25th percentile to 75th percentile distribution. It is seen that the halo gas mass of all quenched samples reached their maximum at an early stage, and they then decrease with redshift. For the star-forming galaxies, their halo gas mass reach the maximum at the present day. This plot also shows that the halo gas mass in SampleQ are lower than that in SampleF, which is consistent with what we have shown in Figure 3.

[10] These unevenly spaced time intervals correspond to the evenly spaced snapshot intervals: [40, 45), [45, 50), [50, 55), [55, 60), [60, 65), [65, 70), [70, 75), [75, 80), [80, 85), [85, 90), [90, 95), [95, 99].
[11] Corresponding to snapshot interval [60, 80).
[12] Corresponding to snapshot interval [80, 99].

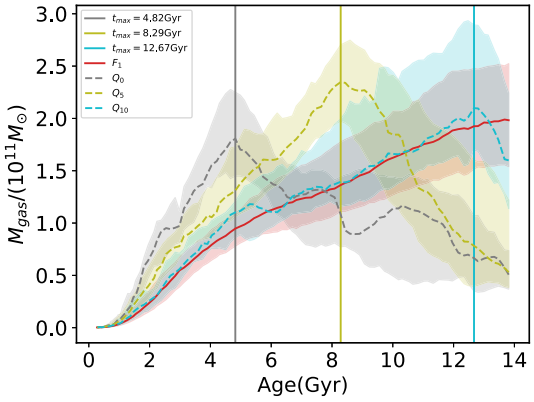

Figure 7. The evolution history of gas mass. The three quenching groups, Q_0, Q_5 and Q_{10}, which correspond to those galaxies that achieved their peak gas mass in the universe age interval [4.29, 5.12) Gyr, [8.28, 9.06) Gyr and [12.34, 13.13) Gyr, correspond to the gray, green and light-blue dashed lines respectively, while the red-solid line represents the star-forming group, $F_1(t_{\max} \in [10.65, 13.80)$ Gyr). The three vertical lines shows the median of $t_{\max}$ for the corresponding quenching groups(with the same color). These values are $t_{\max} = 4.82$ Gyr for Q_0, $t_{\max} = 8.29$ Gyr for Q_5 and $t_{\max}$= 12.67 Gyr for Q_{10}. The 25th percentile to 75th percentile are denoted by the appropriately colored corridors. It is notable that the gas mass of the quenched galaxies increase at first and they then decrease later but for the star-forming galaxies the gas mass always rises.

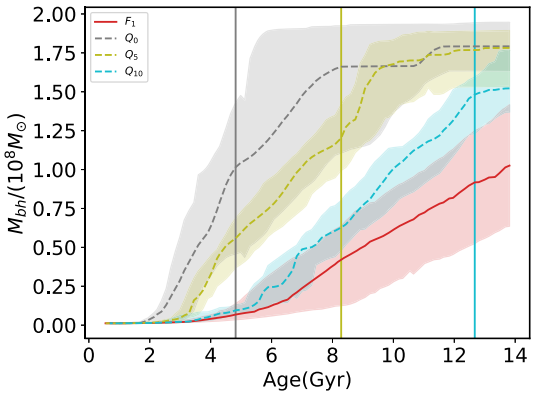

Figure 8. The evolution history of black hole mass. The meaning of the other signs are same as Figure 7. The $M_{\rm bh}$ of the quenched samples grow faster and are larger than the star-forming sample.

4.2. The Evolution of Black Hole Mass

We now show the evolution history of the black hole mass, $M_{\rm bh}$, in Figure 8. All of the notations are same as in Figure 7. The first signature to see is that the three dashed lines are always above the solid line, which means the mass of $M_{\rm bh}$ of the quenched samples grow faster and are larger than the star-forming samples. Among the quenching samples, $M_{\rm bh}$ of subsample with lower $t_{\max}$ (e.g., Q_0) increases more rapidly and reached the threshold ($\sim 10^8\ M_\odot$, above which the feedback from black hole will switch from thermal to kinetic mode) earlier than that of the subsample with larger $t_{\max}$ (e.g., Q_{10}). We can also find that the black hole mass $M_{\rm bh}$ of all three quenched subsamples reached the threshold almost at their own median $t_{\max}$ (i.e., the time when the gas mass begins to decrease, marked by the vertical colored-solid lines). The coincidence of time when the black hole is above the threshold and when the total gas begins to decrease clearly indicates that the kinetic AGN feedback mode transforms a galaxy from star-forming to quenching.

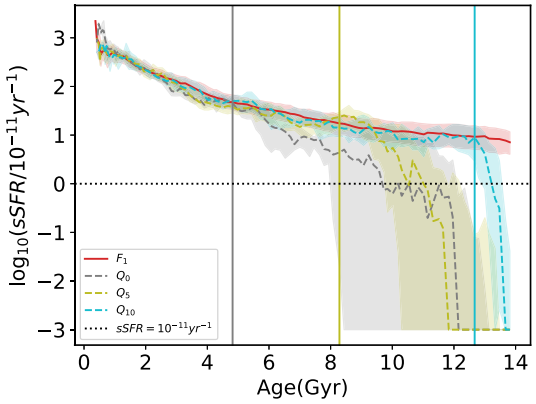

Figure 9. The evolution history of *sSFR*. The meaning of the other notations are the same as Figure 7. It is notable that the dashed lines (quenching groups) decrease more rapidly right after the relevant t_{max}. We set sSFR $= 10^{-14}$ yr^{-1} for galaxies with unresolved SFR (i.e., SFR $= 0\ M_\odot$ yr^{-1}, which is different from the convention used in the Figure 2, just for convenience). The black dotted line is the criterion that is used to distinguish quenched (sSFR $< 10^{-11}$ yr^{-1}) and star-forming (sSFR $> 10^{-11}$ yr^{-1}) galaxies at $z = 0$.

4.3. The Evolution of Specific Star Formation Rates

To further answer whether the decrease of gas mass directly leads to star formation quenching, in Figure 9 we show the evolution of sSFR. The horizontal dotted line is the division for quenching and star-forming. It can be found that the sSFR of the quenched samples (the dashed lines) decreased more rapidly immediately after the corresponding t_{max}, and they will be quenched in $3 \sim 4$ Gyrs. While for star-forming samples (red-solid line), sSFR had a relatively slow decrease and keep a relatively larger value ($>10^{-10}$ yr^{-1}) above the threshold of quenching. This result indicates that the quenching of galaxies in SampleQ is really related to the loss of gas mass. Although some other process, such as stellar feedback or star formation could play an important role in consuming the gas, the comparison of the Q_{10} (dashed-blue line) and F_1 (red-solid line) pointed out that the AGN feedback should play a key role in gas depletion because they had almost same gas mass (see Figure 7) and sSFR evolution (Figure 9) before t_{max}, but with quite different black hole mass evolution (Figure 8). The quenching from the AGN feedback only began to be effective when the galaxies have a central black hole mass above the threshold of $M_{bh} \sim 10^8\ M_\odot$. This conclusion also explains why some galaxies in SampleF with higher black hole mass ($\sim 10^8\ M_\odot$) are still star-forming (i.e., their black hole mass has very recently reached this threshold).

We may conclude that the massive black hole and its effective kinetic feedback could drive a large amount of gas loss, thereby depleting the gas reservoir and thus effectively quenching star formation. In fact, the strong AGN feedback can also suppress gas inflow to halos, which could also decrease the gas mass in halo (e.g., Wright et al. 2020). The overall effect of AGN feedback, either by producing outflow or suppressing inflow, is to decrease the total gas content of the galaxy and in this work we do not distinguish between these two processes.

5. How Did Black Holes Grow in Massive Disk Galaxies?

We have found that the kinetic feedback of the SMBH is the key to quench star formation for massive disk galaxies. We now come to the question: how did the SMBHs grow in these massive disk galaxies? In the classical scenario of bulge-black hole coevolution, the black hole and bulge mainly grow through galaxy mergers. However, this scenario does not seem to apply to the current case (i.e., disk-dominate galaxies with massive SMBH). As mentioned in the introduction, this kind of galaxy does not follow the classical bulge mass-BH mass relationship and their SMBHs mainly grows via non-major-merger processes. In the following section, we investigate how the SMBHs in our samples grow in the simulation.

5.1. The Possible Path of Black Hole Growth

From the black hole growth evolution (Figure 8), we have found that the quenched subsamples have experienced fast growth at the early stage. We further investigate the evolution of the black hole mass accretion rate. Here, the accretion rate is instantaneous black hole mass growth rate given by the TNG simulation. As shown in the Figure 10, during the interval between the open arrow and the solid arrow with the same color code, the SMBHs of all three quenched subsamples kept very high accretion rates ($>10^7\ M_\odot$ Gyr^{-1}) for a period of time, and the accretion rates then decreased rapidly. The star-forming sample (red line) kept relatively lower accretion rates ($\sim 10^{6.5}\ M_\odot$ Gyr^{-1}). The fact that both the quenched and star-forming samples experience such a high-accretion phase for several billion years may suggest that SMBH accretion plays a dominant role in driving the growth of SMBHs in massive disk galaxies. By using TNG300 simulation, Weinberger et al. (2018) obtained the same results as in this work, in which they found that SMBH ($<10^{8.5}\ M_\odot$) mainly grows via accretion.

We also found that for the quenched subsample, the time when the accretion rate of black hole began to decrease is correlated with t_{max} (marked with open arrows). At around t_{max}, when the black hole mass reached the threshold ($\sim 10^8\ M_\odot$), AGN feedback mode is switched from thermal to kinetic, so the surrounding gas is quickly expelled and this leads to a lower accretion rate afterwards.

This black hole growth pattern supports the results from some previous work (McAlpine et al. 2017, 2018, from EAGLE simulation), which indicated that there are three black hole growth phases: the stellar feedback regulated phase, the nonlinear black hole growth phase, and the AGN feedback regulated phase. Bower et al. (2017) found that the switch between the two phases are governed by the halo virial mass. When the halo virial mass is lower than certain critical mass M_{crit}, the mass accretion could be suppressed by the stellar feedback. When the halo virial mass is above the M_{crit}, the black hole would be in nonlinear growth phase. The M_{crit} can be calculated as $M_{crit} = 10^{12}(\Omega_m(1+z)^3 + \Omega_\Lambda)^{-1/8} M_\odot$.

We show the halo virial mass evolution history of all four subsamples, and M_{crit} (black solid line) in Figure 11. We marked the critical time t_{crit} when the median halo virial mass of each subsample exceeds the M_{crit} with colored arrows. For those four subsamples, the t_{crit} are: $t_{crit} = 2.54$ Gyr (for Q_0), $t_{crit} = 3.28$ Gyr (for Q_5), $t_{crit} = 3.9$ Gyr (for Q_{10}), $t_{crit} = 4.5$ Gyr (for F_1).

We also marked these critical times on the evolution of black hole accretion rate using solid arrows in Figure 10. We found that for all the quenched subsamples, the black hole has a high accretion rate during the time between t_{crit} and t_{max} (solid and open arrows in Figure 10, respectively), which well correspond to the nonlinear growth phase. After t_{max}, black hole growth is in the AGN feedback regulated phase. During this phase,

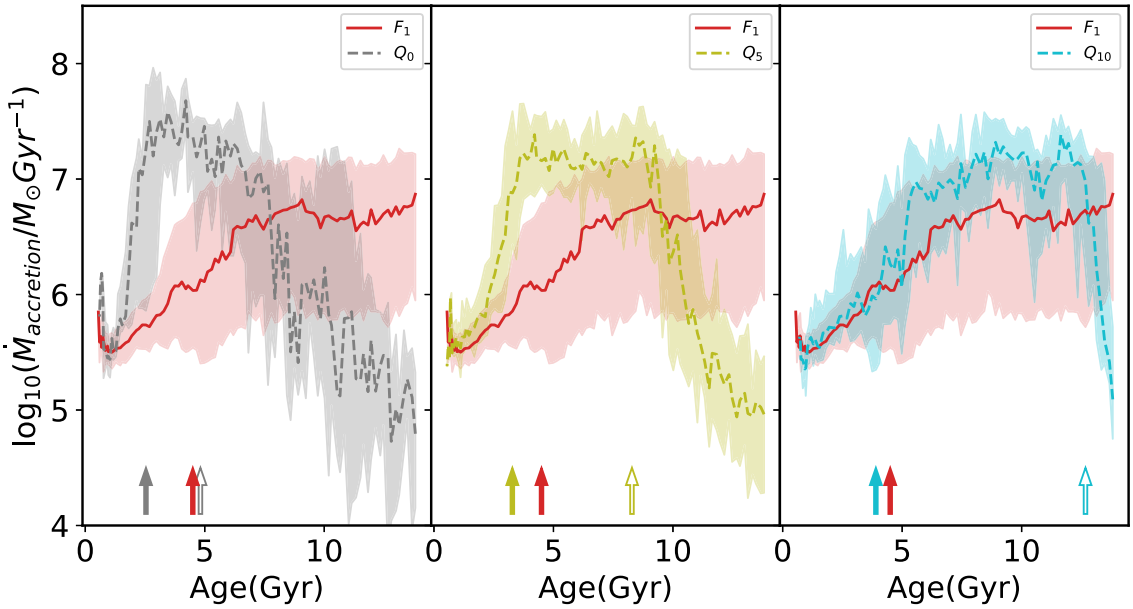

Figure 10. The evolution of black hole accretion rate. From left to right, the black hole mass accretion rate of each quenching sample group have been compared with that of the star-forming group in each panel. We also shown the t_{max} marked with open arrows. The filled arrows have the same meaning as those in Figure 11. Quenched subsamples keep very high accretion rates for a period of time, and the rates then decline rapidly. However, the star-forming sample (red line) keep relatively lower rates, which are more or less constant.

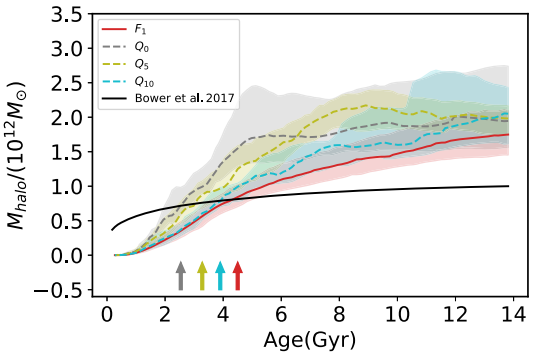

Figure 11. The evolution history of halo virial mass. The meaning of the other notations are the same as those in Figure 7. The black line denotes the evolution of the critical halo virial mass M_{crit}, below which the black hole accretion will be suppressed by the stellar feedback (Bower et al. 2017). The colored arrows represents the earliest snapshot at which the mass of the halo of the corresponding samples are higher than the the critical halo virial mass M_{crit}.

although the accretion rate is lower (in fact, it still could be $>10^5\ M_\odot\ \mathrm{Gyr}^{-1}$), the AGN feedback is still strong enough to decrease the star formation because the kinetic mode is more effective than the thermal mode to remove the surrounding gas. We note that at $z=0$, all of the quenched samples are in the AGN feedback regulated phase, while the star-forming sample is still in the nonlinear black hole growth phase because their black hole mass has just approached the threshold mass ($\sim 10^8 M_\odot$).

5.2. The Evolution History of Morphology and Merger

A key question about quenched disk galaxies is when they are formed. Using the integral field spectroscopy from the SDSS-IV MaNGA sample, the recent study by Zhou et al. (2021b) showed that massive red disk galaxies formed as early as elliptical galaxies, with more than half stellar mass are formed at 10 Gyrs ago. Meanwhile, it is often thought that massive black hole is formed mainly in major merger, under the merger-driven scenario for the coevolution of the black hole and galaxy, but major mergers usually lead to the formation of a massive galactic bulge. Why do these massive disk galaxies lack significant bulge if their massive black hole are formed in major mergers? In the following subsection, we investigate the morphology evolution of these quenched disk galaxies and the role of merger for the formation of the disks.

Along the evolution track of each model galaxy, we decompose their star distribution into bulge and disk using the kinematic method mentioned in Section 2. We then plot the evolution of S/T of quenched subsamples in Figure 12. Here, considering the star mass resolution, we only selected galaxies with more than 1000 particles within $3R_e$ to derive reliable estimate of S/T at every snapshot. It is interesting to see that the median S/T has a low value (<0.25) during the evolution, showing that these quenched massive disk galaxies have disk morphology for a long time. At early times, the scatter is slightly larger, possibly due to the resolution effect (i.e., less star particles at early times) but the scatter of S/T is lower after t_{max}. Zeng et al. (2021) also found that some massive disk galaxies preserve the disk morphology since their formation in TNG simulation. They argued that major mergers with special orbits could produce disk-dominant remnants.

Usually, the formation of the bulge is mainly due to a major merger of galaxies. This long-lasting disk morphology of SampleQ may hint that major merger is not dominant during their formation. Consequently, we study the merger event of our four subsamples. Here, we classify three kinds of mergers according to the merger mass ratio: major merger $\left(\mu \geqslant \frac{1}{3}\right)$, minor merger $\left(\frac{1}{3} > \mu \geqslant \frac{1}{10}\right)$ and mini-merger $\left(\frac{1}{10} > \mu\right)$. The mass ratio, μ, defined as $\mu \equiv \frac{M_{\star,1}}{M_{\star,2}}$, where $M_{\star,1} < M_{\star,2}$ represents stellar mass of two merging galaxies, respectively. (The definition of the mass ratio μ is the same as in Rodriguez-Gomez et al. 2015.) We then calculated the cumulative merger numbers for every galaxy.

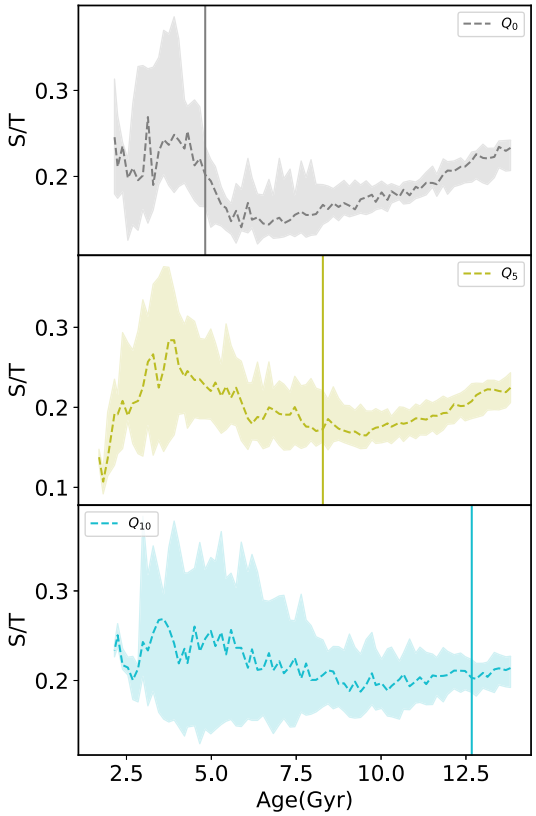

Figure 12. The evolution of the S/T of the quenched groups. From top to bottom, we consider different quenched groups. We only choose the galaxies with at least 1000 star particles to construct the curve at every snapshot. Where the vertical line is the same as the one that is plotted in Figure 7. These curves indicate that quenched massive disk galaxies got disk morphology many billions of years ago.

In Figure 13, we compared the cumulative merger numbers of each subsample for three different merger types separately. As we can see from the first row, all of the samples have at most one major merger at early stage $t < t_{\rm max}$. Interestingly, these major mergers did not quench the star formation of those galaxies (sSFR decreased significantly only after $t_{\rm max}$; see Figure 9). This is consistent with the results of Weinberger et al. (2018) and Park et al. (2021) that a major merger event is not a main cause of quenching in the TNG simulation.

From the second row of Figure 13, it seems that there are no clear distinction between the number of minor mergers between the quenched samples and the star-forming sample. However, for the mini-merger shown in the lowest row, the quenched samples had more frequent mini-merger events. We also marked $t_{\rm crit}$ and $t_{\rm max}$ by the solid and open arrows in the Figure 13. Most of the mini-mergers happened between $t_{\rm crit}$ and $t_{\rm max}$. This is exactly the period when the black hole has a higher accretion rate (i.e., the nonlinear black hole growth phase shown in Figure 10). Furthermore, these frequent mini-mergers nearly did not change the morphology of those galaxies. Hence, we can conclude that the frequent mini-mergers cause the rapid growth of SMBHs in quenched disk galaxies and these mini-mergers did not significantly change the disk morphology of these galaxies. All of the massive disk galaxies in our sample, either quenched or star-forming, have experienced few major mergers. Our conclusion of non-major-merger-driven growth of SMBHs in disk galaxies is consistent with many recent studies (e.g., Kocevski et al. 2012; Kaviraj 2014; Martin et al. 2018; McAlpine et al. 2020).

6. Summary and Conclusion

The recent finding of quenched massive disk galaxies has raised great concern about how they formed and were quenched (e.g., Zhang et al. 2019; Zhou et al. 2021b; Xu et al. 2021; Zhang et al. 2021). Most current work has focused on their observational properties and little attention has been paid to their origins. In this work, we used the IllustrisTNG300-1 simulation to study the formation and quenching of massive ($M_\star > 10^{10.5}\ M_\odot$) disk galaxies in detail.

We selected massive ($M_\star > 10^{10.5}\ M_\odot$) central galaxies at $z = 0$ from TNG. By comparing a quenched sample (sSFR $< 10^{-11}$ yr^{-1} and S/T < 0.25) and a star-forming sample (sSFR $> 10^{-11}$ yr^{-1} and S/T < 0.25), we found that the quenched sample has less total gas and lower hydrogen density but they posses a more massive black hole than the star-forming sample.

We then investigated the evolution history of those massive disk galaxies. We found that for those quenched galaxies, their halo gas mass and sSFR began to decrease when the mass of SMBH reached the threshold ($\sim 10^8\ M_\odot$) where the feedback mode of the SMBH will be changed from thermal to kinetic mode, which is more efficient to expel gas from the galaxy.

We further investigated the accretion history of black hole and found that the black hole accretion rate of quenched samples is higher than star-forming counterparts during the period between $t_{\rm crit}$ and $t_{\rm max}$. This period of high accretion rate corresponds to the nonlinear black hole growth phase. From the evolution of morphology and merger event, we found the quenched galaxies formed their disk when Age(cosmic) $\lesssim t_{\rm max}$ and were able to keep the disk morphology for a long time. Both quenched and star-forming samples lack major mergers. Compared to the star-forming galaxies, the frequent mini-merger ($\mu < \frac{1}{10}$) in quenched galaxies during the time interval ($t_{\rm crit} <$ Age(cosmic) $< t_{\rm max}$) led to the rapid growth of the black hole while preserving their disk morphology.

We can conclude that in the IllustrisTNG simulation, the frequent mini-mergers could make the SMBHs grow rapidly, and the kinetic feedback of black hole produced low cold gas density and finally quenched the massive disk central galaxies.

Under this quenching scenario, we should expect that the massive quenched disk central galaxies will hold a massive black hole and own a low gas fraction($f_{\rm CGM} \equiv \frac{M_{\rm gas}}{M_{200}}$). However, the gas fraction $f_{\rm CGM}$ is not a direct observable. To test our result, we need to find a direct observable accessible with current technologies and telescopes to estimate $f_{\rm CGM}$. Recently, using EAGLE simulations, Oppenheimer et al. (2020) argued that, for $L^\star$ mass ($M_\star = 10^{10.2} - 10^{10.7}\ M_\odot$) central galaxies, the covering fraction, $C_{\rm C_{IV}>13.5,100\,kpc}$, of absorbers C_{IV} with column density $N_{\rm C_{IV}} > 10^{13.5}$ cm^{-2} within an impact parameter 100 kpc is a well observational proxy for $f_{\rm CGM}$. They found that $C_{\rm C_{IV}>13.5,100\,kpc}$ correlates strongly and positively with $f_{\rm CGM}$ (Figure 3 of their paper). More importantly, the C_{IV} 1548, 1551 Å doublet is obtainable via the Cosmic Origins Spectrograph on the Hubble Space Telescope in the local universe. Thus, for local galaxies, the $C_{\rm C_{IV}>13.5,100\,kpc}$ are available and their SMBHs mass are also accessible. We hope that massive and quenched disk galaxies owning low covering

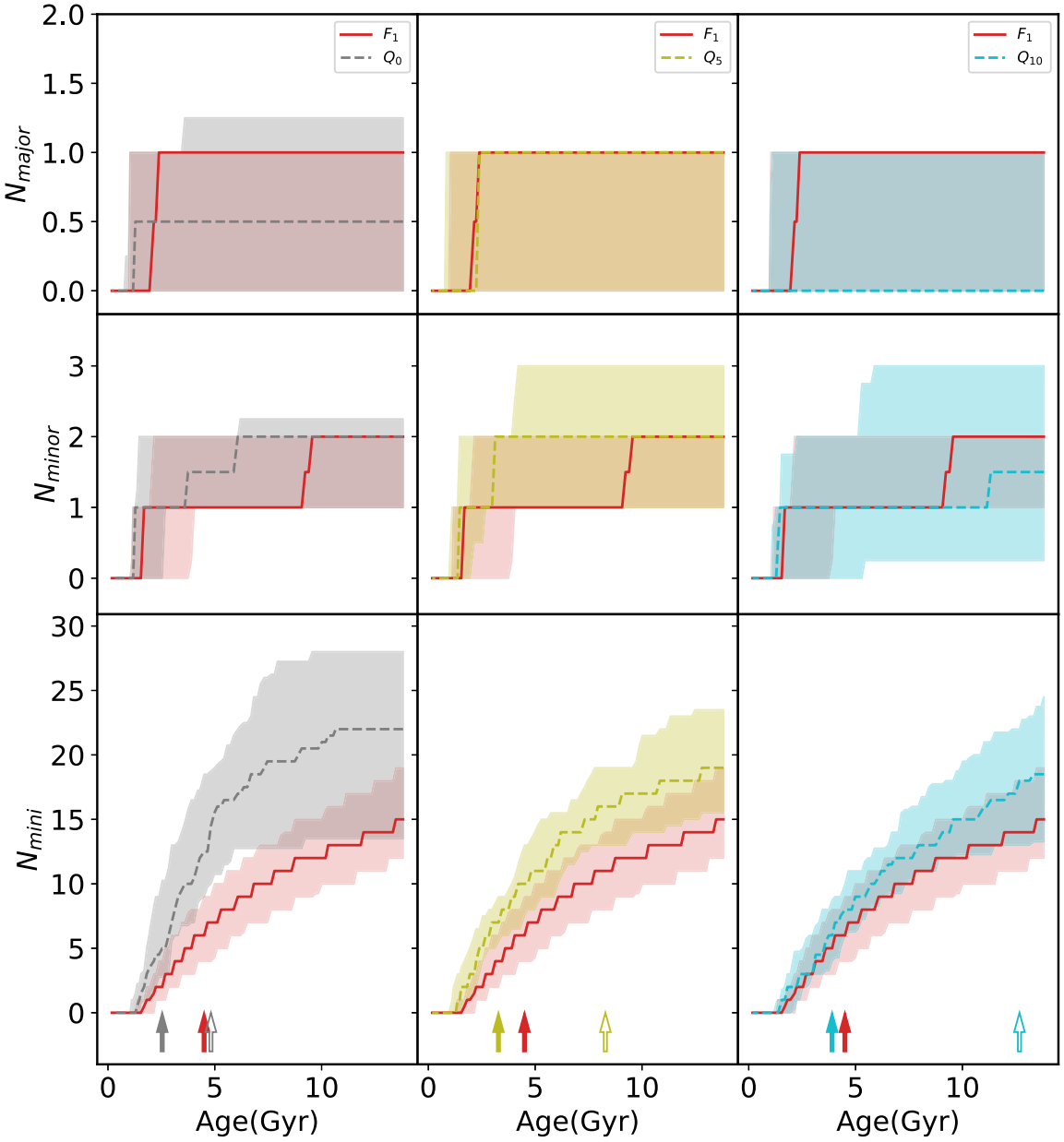

Figure 13. We compare the cumulative merger numbers of each quenched sample and star-forming sample on each column. From top to bottom, we consider three kinds of mergers: major merger$\left(\mu \geqslant \frac{1}{3}\right)$, minor merger$\left(\frac{1}{3} > \mu \geqslant \frac{1}{10}\right)$ and mini-merger$\left(\frac{1}{10} > \mu\right)$. The meaning of the colored arrows is the same as those in Figure 10. All samples have almost one major merger that occurred at very early time. While quenched samples experienced more frequent mini-mergers. As for the minor merger, there is no distinction between the star-forming group and the quenched group.

factor $C_{C_{IV}>13.5,100\ kpc}$ and giant SMBH could be used to test our conclusions.

We thank Yaoxin Chen for the helpful comments. This work is supported by the NSFC (grant Nos. 11861131006, 11825303, 11703091, 11333008) and the 973 program (grant No. 2015CB857003). We acknowledge the science research grants from the China Manned Space project with grant Nos. CMS-CSST-2021-A03, CMS-CSST-2021-A04.

ORCID iDs

Yingzhong Xu (徐英中) https://orcid.org/0000-0003-4823-1898
Yu Luo (於洛) https://orcid.org/0000-0003-2341-9755
Xi Kang (康席) https://orcid.org/0000-0002-5458-4254
Zhiyuan Li (李志遠) https://orcid.org/0000-0003-0355-6437
Zongnan Li (李宗男) https://orcid.org/0000-0002-7172-6306
Peng Wang (王鹏) https://orcid.org/0000-0003-2504-3835
Noam Libeskind https://orcid.org/0000-0002-6406-0016

References

Abadi, M. G., Navarro, J. F., Steinmetz, M., & Eke, V. R. 2003a, ApJ, 597, 21
Abadi, M. G., Navarro, J. F., Steinmetz, M., & Eke, V. R. 2003b, ApJ, 591, 499
Benson, A. J., Bower, R. G., Frenk, C. S., et al. 2003, ApJ, 599, 38
Bizzocchi, L., Filho, M. E., Leonardo, E., et al. 2014, ApJ, 782, 22
Blanton, M. R., Hogg, D. W., Bahcall, N. A., et al. 2003, ApJ, 594, 186
Bohn, T., Canalizo, G., Satyapal, S., & Pfeifle, R. W. 2020, ApJ, 899, 82
Bower, R. G., Benson, A. J., Malbon, R., et al. 2006, MNRAS, 370, 645
Bower, R. G., Schaye, J., Frenk, C. S., et al. 2017, MNRAS, 465, 32
Cattaneo, A., Faber, S. M., Binney, J., et al. 2009, Natur, 460, 213
Cisternas, M., Jahnke, K., Bongiorno, A., et al. 2011, ApJL, 741, L11

Couch, W. J., Barger, A. J., Smail, I., Ellis, R. S., & Sharples, R. M. 1998, ApJ, 497, 188
Crain, R. A., Schaye, J., Bower, R. G., et al. 2015, MNRAS, 450, 1937
Croton, D. J., Springel, V., White, S. D. M., et al. 2006, MNRAS, 365, 11
Davies, J. J., Crain, R. A., McCarthy, I. G., et al. 2019, MNRAS, 485, 3783
Davies, J. J., Crain, R. A., Oppenheimer, B. D., & Schaye, J. 2020, MNRAS, 491, 4462
Davis, B. L., Graham, A. W., & Cameron, E. 2018, ApJ, 869, 113
Davis, B. L., Graham, A. W., & Cameron, E. 2019, ApJ, 873, 85
Di Matteo, T., Springel, V., & Hernquist, L. 2005, Natur, 433, 604
Doménech-Moral, M., Martínez-Serrano, F. J., Domínguez-Tenreiro, R., & Serna, A. 2012, MNRAS, 421, 2510
Fraser-McKelvie, A., Brown, M. J. I., Pimbblet, K., Dolley, T., & Bonne, N. J. 2018, MNRAS, 474, 1909
Ghosh, H., Mathur, S., Fiore, F., & Ferrarese, L. 2008, ApJ, 687, 216
Greene, J. E., Peng, C. Y., Kim, M., et al. 2010, ApJ, 721, 26
Guo, R., Hao, C.-N., Xia, X., et al. 2020, ApJ, 897, 162
Hao, C.-N., Shi, Y., Chen, Y., et al. 2019, ApJL, 883, L36
Hopkins, P. F., Hernquist, L., Cox, T. J., & Kereš, D. 2008, ApJS, 175, 356
Jiang, Y.-F., Greene, J. E., Ho, L. C., Xiao, T., & Barth, A. J. 2011, ApJ, 742, 68
Kang, X., Jing, Y. P., & Silk, J. 2006, ApJ, 648, 820
Kauffmann, G., & Haehnelt, M. 2000, MNRAS, 311, 576
Kauffmann, G., Heckman, T. M., White, S. D. M., et al. 2003a, MNRAS, 341, 33
Kauffmann, G., Heckman, T. M., White, S. D. M., et al. 2003b, MNRAS, 341, 54
Kaviraj, S. 2014, MNRAS, 440, 2944
Kocevski, D. D., Faber, S. M., Mozena, M., et al. 2012, ApJ, 744, 148
Kormendy, J., & Gebhardt, K. 2001, in AIP Conf. Ser. 586, 20th Texas Symposium on Relativistic Astrophysics, ed. J. C. Wheeler & H. Martel (Melville, NY: AIP), 363
Kormendy, J., & Ho, L. C. 2013, ARA&A, 51, 511
Li, Y., Habouzit, M., Genel, S., et al. 2020, ApJ, 895, 102
Luo, Y., Li, Z., Kang, X., Li, Z., & Wang, P. 2020, MNRAS, 496, L116
Mahajan, S., Gupta, K. K., Rana, R., et al. 2020, MNRAS, 491, 398
Man, A., & Belli, S. 2018, NatAs, 2, 695
Marinacci, F., Vogelsberger, M., Pakmor, R., et al. 2018, MNRAS, 480, 5113
Martin, G., Kaviraj, S., Volonteri, M., et al. 2018, MNRAS, 476, 2801
Masters, K. L., Mosleh, M., Romer, A. K., et al. 2010, MNRAS, 405, 783
McAlpine, S., Bower, R. G., Harrison, C. M., et al. 2017, MNRAS, 468, 3395
McAlpine, S., Bower, R. G., Rosario, D. J., et al. 2018, MNRAS, 481, 3118
McAlpine, S., Harrison, C. M., Rosario, D. J., et al. 2020, MNRAS, 494, 5713
McConnell, N. J., & Ma, C.-P. 2013, ApJ, 764, 184
Naiman, J. P., Pillepich, A., & Springel, V. 2018, MNRAS, 477, 1206
Nelson, D., Pillepich, A., & Springel, V. 2018, MNRAS, 475, 624
Nelson, D., Springel, V., & Pillepich, A. 2019, ComAC, 6, 2
Oppenheimer, B. D., Davies, J. J., Crain, R. A., et al. 2020, MNRAS, 491, 2939
Park, M., Tacchella, S., Nelson, E. J., et al. 2021, arXiv:2112.07679
Pillepich, A., Nelson, D., Hernquist, L., et al. 2017, MNRAS, 475, 648
Pillepich, A., Nelson, D., & Hernquist, L. 2018b, MNRAS, 475, 648
Pillepich, A., Springel, V., Nelson, D., et al. 2018a, MNRAS, 473, 4077
Planck Collaboration, Ade, P. A. R., Aghanim, N., et al. 2016, A&A, 594, A13
Poole, G. B., Mutch, S. J., Croton, D. J., & Wyithe, S. 2017, MNRAS, 472, 3659
Rodriguez-Gomez, V., Genel, S., Vogelsberger, M., et al. 2015, MNRAS, 449, 49
Scannapieco, C., White, S. D. M., Springel, V., & Tissera, P. B. 2009, MNRAS, 396, 696
Schawinski, K., Simmons, B. D., Urry, C. M., Treister, E., & Glikman, E. 2012, MNRAS, 425, L61
Schawinski, K., Treister, E., Urry, C. M., et al. 2011, ApJL, 727, L31
Schawinski, K., Urry, C. M., Simmons, B. D., et al. 2014, MNRAS, 440, 889
Schaye, J., Crain, R. A., Bower, R. G., et al. 2015, MNRAS, 446, 521
Sijacki, D., Springel, V., Di Matteo, T., & Hernquist, L. 2007, MNRAS, 380, 877
Simmons, B. D., Smethurst, R. J., & Lintott, C. 2017, MNRAS, 470, 1559
Simmons, B. D., Urry, C. M., Schawinski, K., Cardamone, C., & Glikman, E. 2012, ApJ, 761, 75
Simmons, B. D., Van Duyne, J., Urry, C. M., et al. 2011, ApJ, 734, 121
Simmons, B. D., Lintott, C., Schawinski, K., et al. 2013, MNRAS, 429, 2199
Smethurst, R. J., Simmons, B. D., Lintott, C. J., & Shanahan, J. 2019, MNRAS, 489, 4016
Smethurst, R. J., Simmons, B. D., Coil, A., et al. 2021, MNRAS, 507, 3985
Snyder, G. F., Torrey, P., Lotz, J. M., et al. 2015, MNRAS, 454, 1886
Somerville, R. S., Hopkins, P. F., Cox, T. J., Robertson, B. E., & Hernquist, L. 2008, MNRAS, 391, 481
Springel, V., Di Matteo, T., & Hernquist, L. 2005a, MNRAS, 361, 776
Springel, V., & Hernquist, L. 2003, MNRAS, 339, 289
Springel, V., Pakmor, R., & Pillepich, A. 2018, MNRAS, 475, 676
Springel, V., White, S. D. M., Tormen, G., & Kauffmann, G. 2001, MNRAS, 328, 726
Springel, V., White, S. D. M., Jenkins, A., et al. 2005b, Natur, 435, 629
Tacchella, S., Diemer, B., Hernquist, L., et al. 2019, MNRAS, 487, 5416
Terrazas, B. A., Bell, E. F., Pillepich, A., et al. 2020, MNRAS, 493, 1888
Tojeiro, R., Masters, K. L., Richards, J., et al. 2013, MNRAS, 432, 359
Toomre, A., & Toomre, J. 1972, ApJ, 178, 623
van den Bergh, S. 1976, ApJ, 206, 883
Vogelsberger, M., Genel, S., Springel, V., et al. 2014a, MNRAS, 444, 1518
Vogelsberger, M., Genel, S., Springel, V., et al. 2014b, Natur, 509, 177
Weinberger, R., Springel, V., Hernquist, L., et al. 2017, MNRAS, 465, 3291
Weinberger, R., Springel, V., Pakmor, R., et al. 2018, MNRAS, 479, 4056
Wright, R. J., Lagos, C. d. P., Power, C., & Mitchell, P. D. 2020, MNRAS, 498, 1668
Xu, K., Liu, C., Jing, Y., Sawicki, M., & Gwyn, S. 2021, SCPMA, 64, 279811
York, D. G., Adelman, J., Anderson, J. E. J., et al. 2000, AJ, 120, 1579
Zeng, G., Wang, L., & Gao, L. 2021, MNRAS, 507, 3301
Zhang, C., Peng, Y., Ho, L. C., et al. 2019, ApJL, 884, L52
Zhang, C., Peng, Y., Ho, L. C., et al. 2021, ApJ, 911, 57
Zhou, R., Newman, J. A., Mao, Y.-Y., et al. 2021a, MNRAS, 501, 3309
Zhou, S., Li, C., Hao, C.-N., et al. 2021b, ApJ, 916, 38
Zinger, E., Pillepich, A., Nelson, D., et al. 2020, MNRAS, 499, 768